Modulation format dependence on transmission reach in phase-sensitively amplified fiber links

Citation for the original published paper (version of record):
Vijayan, K., He, Z., Foo, B. et al (2020). Modulation format dependence on transmission reach in phase-sensitively amplified fiber links. Optics Express, 28(23): 34623-34638.
http://dx.doi.org/10.1364/OE.403475

Research Article | Vol. 28, No. 23 / 9 November 2020 / Optics Express 34623
Optics EXPRESS

Modulation format dependence on transmission reach in phase-sensitively amplified fiber links

KOVENDHAN VIJAYAN,[1,*] ZONGLONG HE,[1] BENJAMIN FOO,[2] MAGNUS KARLSSON,[1] AND PETER A. ANDREKSON[1]

[1] *Photonics Laboratory, Department of Microtechnology and Nanoscience, Chalmers University of Technology, SE-412 96 Gothenburg, Sweden*
[2] *Infinera Corporation, 7360 Windsor Drive, Allentown, PA 18106, USA*
[*] *vijayan@chalmers.se*

Abstract: We quantify the maximum transmission reach for phase-insensitive amplifier (PIA) and phase-sensitive amplifier (PSA) links with different modulation formats and show that the maximum transmission reach increase (MTRI) when using PSAs compared to PIAs is enhanced for higher-order modulation formats. The higher-order modulation formats are more susceptible to smaller phase rotations from nonlinearities, and PSAs are efficient in mitigating these smaller phase distortions. Numerical simulations were performed for single- and multi-span PIA and PSA links with single and multiple wavelength channels. We obtain a significant enhancement in the MTRI with PSAs compared to PIAs when using higher-order modulation formats for both the single- and multi-channel systems in single- and multi-span links. We verify the enhancement with a single-span, single-channel system experiment. We also demonstrate, for the first time, a 64-QAM modulation format fiber transmission in phase-sensitively amplified link, with a 13.3-dB maximum allowable span loss increase compared to a phase-insensitively amplified link.

1. Introduction

The transmission reach in optical communication systems is fundamentally limited by the noise added by the optical amplifiers. In systems with linear transmission medium, the noise limitation can be overcome by simply increasing the power. However, in fiber-optic communication systems, nonlinear distortions caused by the Kerr effect in the fiber at high powers limit the maximum power that can be launched into the fiber and thus the reach [1,2]. The nonlinear distortions are, to some extent, deterministic, and several techniques have been used to mitigate these nonlinear distortions. Some digital techniques widely studied are digital back-propagation (DBP) [3,4] and nonlinear Fourier transform (NFT) [5]. In DBP, the signal is virtually back-propagated after detection to compensate for dispersion and nonlinearities. A nonlinear spectrum is transmitted to make the Kerr effect beneficial rather than detrimental in the NFT. Phase-conjugated twin waves (PCTWs) [6,7] is one other technique in which the signal and conjugated copy of the signal known as idler are propagated together through the optical fiber experiencing correlated nonlinear distortions. After detection, the nonlinear distortions are canceled by coherently combining the signal and idler in the digital domain at the receiver. All-optical techniques include the optical phase conjugations (OPCs) [8,9] and phase-sensitive amplifiers (PSAs) [10]. In OPCs, the signal is phase conjugated at the center of the span, also known as mid-span spectral inversion, to reverse the effects of even order dispersion and nonlinearities.

PSAs based on the copier-PSA scheme [11] are very similar to PCTWs. The copier is used to generate the idler. The signal and idler copropagate in the transmission span, where they experience correlated nonlinear distortions. A highly nonlinear medium acts as the PSA after the span. Through the process of parametric amplification, the signal and idler are added coherently in the optical domain with frequency and phase locking, enabling nonlinearity mitigation. The coherent addition of the optical fields also provides a 0-dB quantum-limited noise figure (NF)

#403475 https://doi.org/10.1364/OE.403475
Journal © 2020 Received 27 Jul 2020; revised 27 Sep 2020; accepted 30 Sep 2020; published 2 Nov 2020

Optics EXPRESS

compared to a 3-dB NF for phase-insensitive amplifiers (PIAs) [12]. Therefore, copier-PSAs are capable of mitigating nonlinearities while simultaneously amplifying the signal without adding excess noise. However, the drawback is that PSAs require a conjugated copy of the signal, which reduces the spectral efficiency. Copier-PSAs can be implemented using two-mode (different signal and idler frequencies) parametric amplifiers [13,14] in $\chi^{(3)}$ platforms based on four-wave mixing (FWM). In $\chi^{(2)}$ media, cascaded second-order nonlinear effects can be used to implement copier-PSAs [15]. A copier-PSA using highly nonlinear fibers (HNLFs), which is a $\chi^{(3)}$ nonlinear medium, has been demonstrated to have a low NF of 1.1 dB [16]. PSAs, in general, are capable of amplifying only single-polarization (SP) signals. However, dual-polarization (DP) signals can be amplified with either polarization-diverse PSAs [17,18] or vector PSAs [19,20].

In a single-channel fiber-optic communication link, the nonlinear distortions are mainly caused by signal-to-signal interaction within the same channel known as self-phase modulation (SPM). Both SPM and cross-phase modulation (XPM) contribute to the nonlinear phase distortions in multi-channel fiber systems. The XPM is caused by the signal-to-signal interactions between two different channels. XPM is the dominant nonlinear effect when having multiple channels at lower baud rates [21], considering only single-polarization signals and dispersion-managed links. PSAs are capable of mitigating both the SPM [10] and XPM [22]. Though the legacy optical fiber communication links are spanwise dispersion managed, the introduction of coherent detection and the advancement in the digital signal processing (DSP) in recent times lead to compensating dispersion digitally after detection. The possibility of digital dispersion compensation after detection removed the need for inline spanwise optical dispersion compensation modules in the fiber links. Moreover, the negative impact of the nonlinear effects on system performance can be reduced by not having inline spanwise dispersion compensation modules. Therefore, the dispersion-unmanaged (DU) links are interesting while studying the limits imposed by nonlinearities in a multi-span scenario.

Under certain assumptions, the best achievable spectral efficiency of optical transmission links is given by the Shannon-Hartley theorem [23] known as the Shannon limit. By using M-quadrature amplitude modulation (M-QAM) and increasing the M, i.e., using higher-order modulation formats, the spectral efficiency can be pushed towards the Shannon limit. However, higher-order modulation formats are more susceptible to noise. In addition, small phase rotations can result in more errors for higher-order modulation formats. Moreover, the maximum transmission reach at optimal launch power depends on the nonlinearity in the system, and the amount of nonlinearity that the system can tolerate. Phase-sensitively amplified fiber transmission links utilizing the copier-PSA scheme with 4-QAM [24,25], and 16-QAM [26–28] signals have been experimentally demonstrated. However, there is no study comparing the maximum transmission reach increase (MTRI) when using PSAs instead of PIAs for different modulation formats. This study aims to fill that void.

In this paper, we show that the MTRI is enhanced when using PSAs instead of PIAs with higher-order modulation formats numerically for single- and three-channel systems in single- and multi-span links. Simulations were performed for a single- and three-channel, single- and multi-span PIA and PSA links using 4-, 16-, 64-, and 256-QAM. For both single- and multi-span links, MTRI enhancement with higher-order modulation formats was obtained. We also verify the MTRI enhancement with higher-order modulation formats experimentally with the single-span, single-channel system, which was already reported in [29]. We measure the maximum allowable span loss (MASL) increase for 4-, 16-, and 64-QAM modulation formats as 7.7, 10.8, and 13.3 dB, respectively. To the best of our knowledge, for the first time, we demonstrate a single-channel 64-QAM modulation format transmission over a single span of fiber with PSAs as a preamplifier. The enhancement in the MTRI for higher-order modulation formats is due to the effective mitigation of smaller nonlinear distortions in PSAs [10] as higher-order modulation formats are more susceptible to smaller phase rotations. The transmission reach corresponding to BER of

Optics EXPRESS

$2x10^{-3}$ was considered for the simulations and experiments as the forward error correction (FEC) can reduce a BER of $2x10^{-3}$ to 10^{-12} [30] with ~7% overhead.

This paper is organized as follows: in section 2, the copier-PSA link's working principle is elaborated, showing how copier-PSAs can mitigate nonlinearities while simultaneously providing low-noise amplification. The numerical simulation for both single- and multi-span PIA and PSA links with 4-, 16-, 64-, and 256-QAM are included in section 3, validating the enhancement in the MTRI when using PSAs compared to PIAs. In section 4, the enhancement is experimentally verified with a single-channel, single-span experiment. Section 5 contains the discussion on the results, and the paper is concluded in section 6.

2. Phase-sensitive parametric optical amplifiers and nonlinearity mitigation

In this study, we use HNLFs as the highly nonlinear media for implementing copier-PSAs. Parametric amplification can be achieved in the HNLFs through the process of FWM based on $\chi^{(3)}$ nonlinearities. An illustration of the copier-PSA transmission system is shown in Fig. 1. First, the high power pump at frequency ω_P, is combined with the data signal of frequency ω_S and fed into the copier. In the copier through the process of degenerate pump FWM, a new wave called the idler is generated at frequency $\omega_I = 2\omega_p - \omega_S$, which is the conjugated copy of the signal. The generated idler has the exact phase and frequency relationship with the pump and signal to achieve phase-sensitive operation in the second HNLF. The pump, signal, and idler are copropagated in the span. The signal and idler experience correlated nonlinear distortions in the transmission span. The high power pump is attenuated before being launched into the span to avoid nonlinear effects in the transmission fiber, i.e., FWM between pump, signal, and idler. The weak pump is used as the pilot to regenerate the high power pump required for phase-sensitive operation in the PSA through optical injection locking [31,32] at the pump recovery. At the PSA input, the signal and the idler symbols need to overlap temporally, which requires dispersion compensation. Therefore, copier-PSA transmission spans must be dispersion managed. Also, a phase-locked loop (PLL) is required to lock the pump, signal, and idler waves to achieve phase-sensitive operation. In the PSA, the degenerate pump FWM performs the coherent superposition of the signal and idler apart from parametric amplification, which enables transmission span nonlinearity mitigation. After the PSA, the signal is filtered and sent to the receiver.

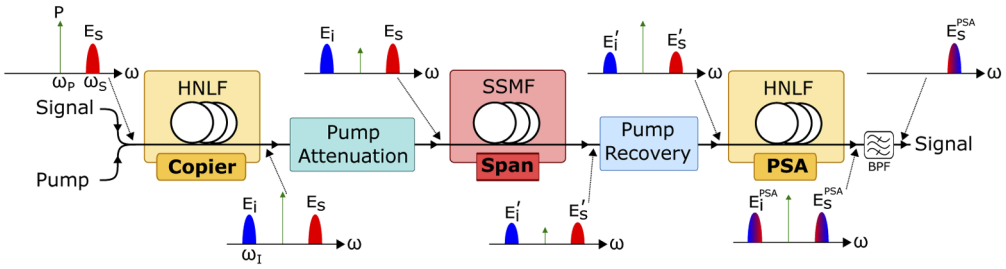

Fig. 1. A simple illustration of a copier-PSA transmission system with the optical spectrum at different points: HNLF - Highly nonlinear fiber, SSMF - Standard single-mode fiber, BPF - Optical bandpass filter.

The coherent superposition of the signal and idler fields also increases the gain by four times of that of the phase-insensitive parametric amplifiers, i.e., PIAs. This leads to low-noise amplification with a theoretical NF of 0 dB [12,16]. At given low launch powers, i.e., in the linear regime, low-noise amplification leads to a 6-dB sensitivity improvement when using PSAs compared to PIAs in single-span PSA links and four times longer reach in multi-span links

Optics EXPRESS

for arbitrary modulation formats. The principle 6-dB sensitivity improvement in single-span PSA fiber links have been demonstrated with single [10,24] and multiple [22,33] channels. In multi-span links, four times higher reach has been obtained for PSAs compared to PIAs in single- [25,27] and multi-channel [34] systems. For a single-channel and single-span system, a signal launch power increase when using PSAs compared to PIAs of 3 dB was estimated with 4-QAM in [35] from nonlinearity mitigation. A 12-dB increase in the MASL was expected in [10] for 16-QAM from nonlinearity mitigation and low-noise amplification.

The complex fields of the signal and idler after the copier are E_S and E_I, respectively where $E_I = E_S^*$. If we neglect dispersion, the nonlinear effects can be modeled as power-dependent phase rotations, $\delta\theta$. The power-dependent phase rotations are made from constant nonlinear phase shift caused by the average signal power, $\delta\theta_{NLPS} = \gamma \overline{P}_S L_{eff}$, and the nonlinear distortions caused by the time-varying fluctuations in the optical power of the signal around its average value, $\delta\theta(t) = \gamma L_{eff}(\overline{P}_S - P_S(t))$, where γ is the fiber nonlinear coefficient, $\overline{P}_S$ is the average signal power and L_{eff} is the effective length. These fluctuations can be caused by noise and multiple amplitude levels in the signal. For modulation formats with a single-amplitude level, the noise is the only source of nonlinear distortions, as in the case of 4-QAM. For higher-order modulation formats, the different amplitude levels along with the noise lead to nonlinear distortions. Also, the higher amplitude signal experiences stronger phase distortion compared to the lower amplitude signals. The constant nonlinear phase shift can be removed by using a carrier phase recovery algorithm in the digital signal processing (DSP) at the receiver, but the nonlinear distortions cannot be removed. Coherent superposition can remove the constant nonlinear phase shift, thanks to the phase-locked loop (PLL) and reduce the nonlinear distortions on the signal [6]. Therefore, we neglect the constant nonlinear phase shift in this analysis. If the signal and idler experience the same power-dependent phase rotations, the nonlinear distortions on the signal and idler are mostly anti-correlated. The signal and idler electric fields after propagation in the transmission span with zero dispersion can be written as

$$E_S^{'} = E_S \exp(-j\delta\theta),$$

$$E_I^{'} = E_I \exp(-j\delta\theta) = E_S^* \exp(-j\delta\theta).$$

Coherent addition takes place in the PSA and the signal field after the PSA is given by

$$E_S^{PSA} = E_S^{'} + (E_I^{'})^* = 2E_S \cos(\delta\theta).$$

Note that the phase fluctuation is absent. PSA reduces the signal field by the cosine of the nonlinearity induced phase distortion, converting them to amplitude distortions,

$$\delta A = 2E_S[1 - \cos(\delta\theta)].$$

On Taylor expanding the above equation, the amplitude distortions become proportional to the square of the nonlinear distortion,

$$\delta A \approx 2E_S[1 - (1 - \frac{(\delta\theta)^2}{2})] = E_S(\delta\theta)^2.$$

For smaller phase distortions, the amplitude distortions caused by the PSAs are also small, showing that PSAs are more effective in mitigating smaller nonlinear phase distortions. For considerable nonlinear phase distortions, substantial amplitude distortions are produced. Also, the different nonlinear phase distortions are converted to various amplitude distortions leading to nonlinear phase-distortion based gain and NF for the PSA [10].

To illustrate the nonlinearity mitigation dependence on the modulation formats when using PSAs, we performed a numerical study with the error-vector magnitude (EVM). Root-raised

Optics EXPRESS

cosine (RRC) shaped 10-GBaud symbols with a roll-off of 10% were transmitted as the signal in an 80-km dispersionless fiber. The signal-to-noise ratio (SNR) at the fiber input was set to values which correspond to BER = 10^{-9} for different modulation formats, and the launch power was varied. No additional noise was added in this study. The signal EVM was calculated after propagation in the fiber and plotted versus the launch power with solid lines and circles in Fig. 2 (left). Red, blue, green, and yellow colors represent 4-, 16-, 64-, and 256-QAM, respectively. At low launch powers (linear regime), the EVMs remained constant. As the launch power was increased (nonlinear regime), the EVMs also increased due to the penalties from nonlinearities. As we move higher in modulation formats, the increase in EVMs arises for lower powers, indicating that the higher-order modulation format is more susceptible to nonlinear distortions. The conjugated copy of the signal was also propagated in an identical fiber as the signal. Coherent superposition of the signal and idler were performed to emulate nonlinearity mitigation in PSAs, and then the signal EVM was calculated. The dotted lines and squares represent the signal EVM after coherent superposition. For the same modulation format, the signal EVM after coherent superposition increases at higher launch powers compared to the signal after propagation due to nonlinearity mitigation. The shaded area corresponds to the less than 1-dB EVM penalty compared to the EVM in the linear regime between the after propagation and after coherent superposition curves. The effectiveness of nonlinearity mitigation is thus given by the shaded region. The increase in the shaded area with higher-order modulation formats suggests that the PSAs can more effectively mitigate penalties caused by nonlinearities in higher-order modulation formats. The constellation diagrams after propagation and after coherent superposition are shown in the top and bottom rows, respectively, in Fig. 2 (right) for different modulation formats. The highest launch powers after coherent superposition with ~0.5-dB EVM penalty were chosen for the different modulation formats. The constellations after propagation and after coherent superposition are shown for 4-, 16-, 64-, and 256-QAM from left to right in Fig. 2 (right). We can see that the nonlinear distortions depend on the amplitude levels. The outermost constellation points with the highest amplitudes have the largest nonlinear distortion and vice versa. The nonlinearity mitigation in PSAs is evident when comparing the constellations after propagation and after coherent superposition. Moreover, zero fiber dispersion was assumed in the above study. In real optical fiber communication links, the dispersion should also be considered to account for the temporal changes in the pulse shape on propagation.

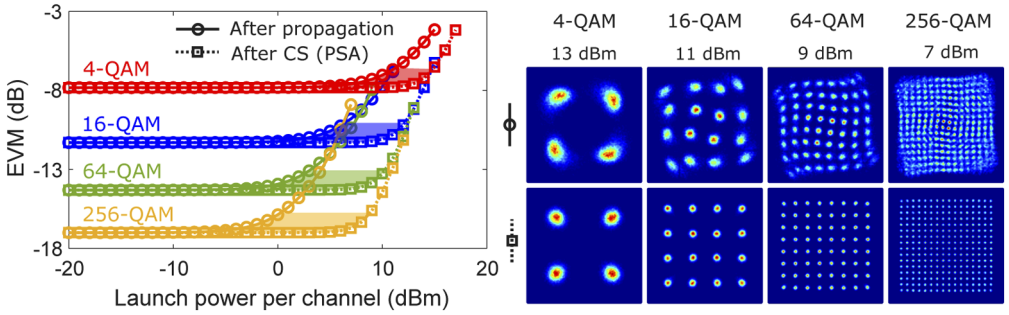

Fig. 2. Left: EVM versus the launch power for different modulation formats after propagation in the fiber with zero dispersion and after coherent superposition (CS). Right: Constellation diagrams after propagation (top) and after CS (bottom) for different modulation formats and launch powers.

Optics EXPRESS

3. Numerical investigation

3.1. Simulation model

To study the modulation-format dependence on the MTRI when using PSAs compared to PIAs, numerical simulations of nonlinear propagation in fibers were performed using MATLAB. The simulation model is shown in Fig. 3. Fiber transmission systems with single and three channels in a single- and multi-span link utilizing single-polarization 4-QAM, 16-QAM, 64-QAM, and 256-QAM 10-GBaud signals were studied. Each channel contained 2^{16} symbols generated from random data and was shaped with RRC filters of 10% roll-off. The symbols were upsampled to 16 samples per symbol for a single-channel system and 32 samples per symbol for the three-channel system before combining. The back-to-back (B2B) SNR was set to 37 dB by adding additive white Gaussian noise (AWGN) to model the experimental transmitter imperfections. The channels were separated by 12.5 GHz in the three-channel system. The required launch powers were set with the booster EDFA, which had an NF of 4 dB. The idler was obtained by perfect conjugation of the signal after the booster EDFA. The transmission span was a 80 km standard single-mode fiber (SSMF) with the fiber loss parameter, $\alpha = 0.2$ dB/km, the dispersion parameter, $D = 16$ ps/nm/km, and the nonlinear coefficient $\gamma = 1.3$ rad/W/km. The propagation in the SSMF was modelled using the split-step Fourier method based on the scalar nonlinear Schrödinger equation (NLSE) [36]. In the experimental implementation of the PSA, the signal and idler were separated by 8 nm. Therefore, the signal and idler were propagated separately in two different split-step solvers as there will not be significant nonlinear XPM interactions between them due to the walk-off. However, for multi-span links in some cases, the XPM interactions between the signal and idler might not be negligible and should be accounted for by copropagating the signal and idler in the same split-step solver. Also, we assumed that the fiber parameters are not wavelength dependent, and the same fiber parameters were used for both the signal and idler split-step solvers for simplicity. As mentioned above, the copier-PSA transmission link should be dispersion managed (DM). Two ideal dispersion compensation modules (DCMs) with $\alpha = 0$ and $\gamma = 0$, one before and one after the span were used to do dispersion pre- and post-compensation. The ratio of the pre- and post-dispersion compensation was optimized for all PIAs and PSAs numerically for the best link performance. The optimization of the pre- and post-dispersion compensation ratio is critical for PSA links compared to PIA links. For the single-channel system, the optimum ratio of pre- to post-dispersion compensation was found to be 24.8% whereas it was 16.3% in the case of the three-channel system for all the modulation formats in the PSA case. Two variable optical attenuators (VOA) were used, one for the signal and the other for the idler to induce any additional loss if needed. Phase noise in the lasers were assumed to be zero.

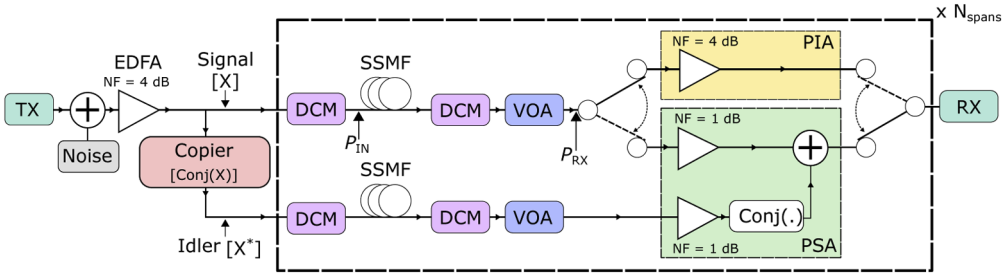

Fig. 3. Simulation model for the single- and multi-span phase-insensitive amplifier (PIA) and phase-sensitive amplifier (PSA) links with single and multiple channels: Tx - Transmitter, EDFA - Erbium-doped fiber amplifier, DCM - Dispersion compensation module, SSMF - Standard single-mode fiber, VOA - Variable optical attenuator, RX - Receiver.

Optics EXPRESS

The signal was amplified after propagation in the span by an EDFA with an NF of 4 dB for PIA. For the PSAs, the signal and idler were separately amplified by two EDFAs with an NF of 1 dB. After amplification, the signal and idler were combined coherently similar to the PSA emulations in the previous works [10,34]. Then, only the signal was sent to the receiver for detection and DSP. In the electrical domain, after matched filtering, the signal was downsampled to 2 samples per symbol. For the three-channel system, the channels were electrically demultiplexed with brick wall filters before downsampling. In the case of the 4-QAM, a constant modulus algorithm (CMA) was used for equalization, whereas for higher-order modulation formats, decision-directed-least-means-squared (DD-LMS) algorithm was used along with CMA for preconvergence. After equalization, the symbols were downsampled to one sample per symbol. Then, the Viterbi-Viterbi phase recovery algorithm was used for carrier phase recovery to compensate for the constant nonlinear phase shift for PIAs. The symbols were then demapped to bits, and the BER was calculated comparing the received bits to the transmitted bits.

Assuming that the signal after propagation in 80-km SSMF is too weak for significant nonlinear interactions, the VOA was used to emulate additional losses that would be caused by the SSMF for longer single-span links. For multi-span links, the attenuation in the VOA was set to zero and the section in the dotted box was repeated for each span. Also, the nonlinear phase noise was present in the simulations due to the inline amplifier noise. For dispersion-unmanaged (DU) PIA links, D was set to zero in the DCMs, and the dispersion was compensated in the digital domain after detection using electrical dispersion compensation (EDC). The launch power (P_{IN}) and the received power (P_{RX}) correspond to only the signal powers.

3.2. Simulation results

The launch power (P_{IN}) was swept, and the transmission reach was measured in terms of allowable span loss in single-span links and length of SSMF traversed in multi-span links. For each of the P_{IN} in the single-span link, the minimum received power (P_{RX}) to reach a BER of $2\mathrm{x}10^{-3}$ called the sensitivity, was obtained. The required P_{RX} was set using the VOA emulating the additional span loss. Then, the allowable span loss was calculated from the difference between the P_{IN} and sensitivity.

The P_{IN} is plotted versus the allowable span loss with one and three channels in Fig. 4(a) and 4(b), respectively using PIAs and PSAs as preamplifiers for different modulation formats. Increasing the P_{IN}, the allowable span loss increases as the sensitivity remains the same. As the nonlinearities start to dominate, a penalty is added to the sensitivity. Then, the allowable span loss starts to decrease with increasing P_{IN}. The MASL can be obtained corresponding to the optimum launch power (OLP) for the PIAs and PSAs. PSAs have higher MASL than PIAs due to low-noise amplification and nonlinearity mitigation. The OLP increase was calculated from the difference between the OLP of the PSA and PIA. The difference between the MASL in the PSA and PIA lead to the MASL increase. The OLP increase and the MASL increase are marked in the corresponding subfigures in Fig. 5 for single- and three-channel systems. Also, Table 1 contains the summary of the single-span link with one and three channels. The nonlinearities are dominated by SPM for a single-channel system, whereas XPM is the predominant one in the three-channel system. The minimum span loss of 16 dB from the 80 km SSMF and the XPM made it impossible to observe the PIA in the linear regime for 256-QAM when using three channels at BER = $2\mathrm{x}10^{-3}$. Therefore, single-span 256-QAM three-channel study is not included in this work. At -5 dBm P_{IN}, for all the 7 cases, comparing the allowable span loss of PSA and PIA, an allowable span increase of 6 dB is obtained. This confirms the low-noise amplification in the linear regime [16]. For all the modulation formats with one and three channels, low noise amplification contributes 6 dB to the MASL increase, and the remaining is dictated by nonlinearity mitigation, which is evident from the OLP increase. Therefore, the MASL increase and OLP increase is enhanced for both the single- and multi-channel systems

Optics EXPRESS

when using higher-order modulation formats in single-span links due to better nonlinearity mitigation.

Table 1. Summary for the single-span link simulations: PIA - Phase-insensitive amplifier, PSA - Phase-sensitive amplifier, OLP - Optimum launch power, MASL - Maximum allowable span loss, OLP increase = $OLP_{PSA} - OLP_{PIA}$, MASL increase = $MASL_{PSA} - MASL_{PIA}$.

Channels	Modulation format	PIA		PSA		OLP increase (dB)	MASL increase (dB)
		OLP (dBm)	MASL (dB)	OLP (dBm)	MASL (dB)		
1	4-QAM	10.5	57.9	12.5	66.4	2.0	8.5
	16-QAM	7.0	46.9	10.5	57.1	3.5	10.2
	64-QAM	3.5	37.2	9.0	49.4	5.5	12.2
	256-QAM	0.0	25.9	7.5	40.3	7.5	14.4
3 (center)	4-QAM	5.5	53.0	8.0	61.5	2.5	8.5
	16-QAM	1.5	41.7	5.5	52.3	4.0	10.6
	64-QAM	-2.0	31.3	4.0	43.3	6.0	12.0
3 (edge)	4-QAM	6.5	53.6	8.5	62.0	2.0	8.4
	16-QAM	2.5	42.2	6.5	52.8	4.0	10.6
	64-QAM	-1.0	31.9	4.5	44	5.5	12.1

For the multi-span links, PIA links without inline dispersion compensation were also studied. The dispersion was not compensated for each span but instead was accumulated and compensated electrically after detection. PIAs without spanwise dispersion compensation are labelled as DU-PIA links in this work. The transmission reach versus P_{IN} for different modulation formats when using PSAs, PIAs, and DU-PIAs with single and three channels is plotted in Fig. 6(a) and 6(b), respectively. Through interpolation, the transmission reach was obtained in the distance transversed for BER = $2x10^{-3}$. The optimum launch power (OLP) and maximum transmission

Table 2. Summary for the multi-span link simulations: PIA - Phase-insensitive amplifier, DU-PIA - Dispersion-unmanaged PIA, PSA - Phase-sensitive amplifier, MTRI - Maximum transmission reach increase

Channels	Modulation format	Maximum transmission reach (km)			MTRI	
		PIA	DU-PIA	PSA	PSA/PIA	PSA/DU-PIA
1	4-QAM	9736	14432	64968	6.7	4.5
	16-QAM	2870	3477	33112	11.5	9.5
	64-QAM	921	940	14968	16.3	15.9
3 (center)	4-QAM	5545	13936	23776	4.3	1.7
	16-QAM	1574	3219	7252	4.6	2.3
	64-QAM	470	702	2202	4.7	3.1
3 (edge)	4-QAM	6090	13640	26920	4.4	2.0
	16-QAM	1670	3166	8104	4.9	2.6
	64-QAM	504	749	2502	5.0	3.3

reach obtained from the different configurations of multi-span links are summarized in Table 2. PSAs have higher maximum transmission reach than PIAs and DU-PIAs due to low-noise amplification and nonlinearity mitigation. In the DU-PIA links, as dispersion is not compensated spanwise, less nonlinear penalties are induced. Therefore, DU-PIAs have higher maximum transmission reach than PIAs and higher optimum launch powers compared to the PIA or PSA links. The MTRI was calculated from the ratio of the transmission reach for PSA and PIA

Optics EXPRESS

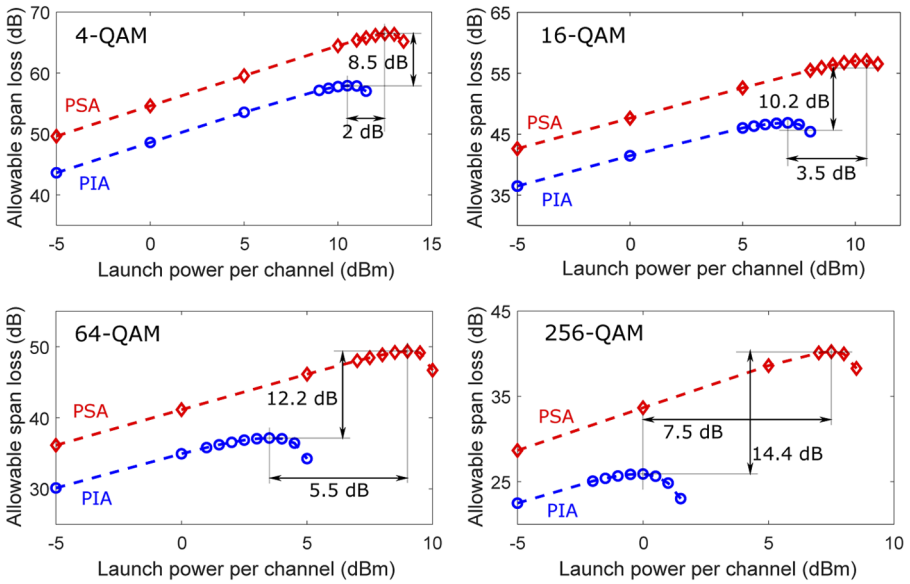

(a) Single-channel system - The dashed blue lines with circle markers and the dashed red lines with diamond markers correspond to phase-insensitive amplifier (PIA) and phase-sensitive amplifier (PSA) links, respectively. The top-left figure is for 4-QAM, top-right for 16-QAM, bottom-left for 64-QAM, and the bottom-right for the 256-QAM. The vertical and horizontal lines with arrows indicate the maximum allowable span loss (MASL) and optimum launch power (OLP) increase, respectively.

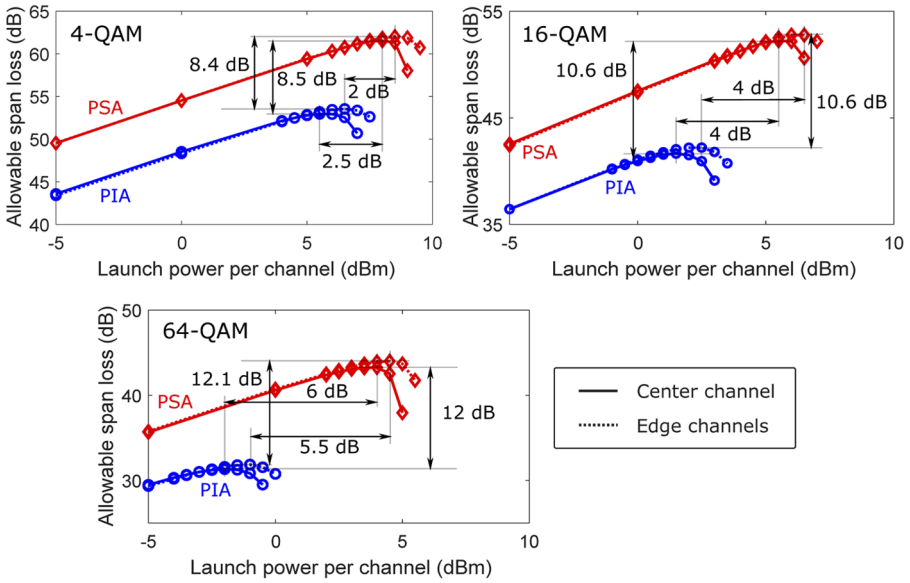

(b) Three-channel system - The blue lines with circle markers and the red lines with diamond markers correspond to phase-insensitive amplifier (PIA) and phase-sensitive amplifier (PSA) links, respectively. The dotted lines represent the edge channels, and the solid lines represent the center channel. The top-left figure is for 4-QAM, top-right for 16-QAM, and the bottom for the 64-QAM. The vertical and horizontal lines with arrows indicate the maximum allowable span loss (MASL) and optimum launch power (OLP) increase, respectively.

Fig. 4. Simulation results - Allowable span loss versus the launch power, P_{IN} for the single-span links.

Optics EXPRESS

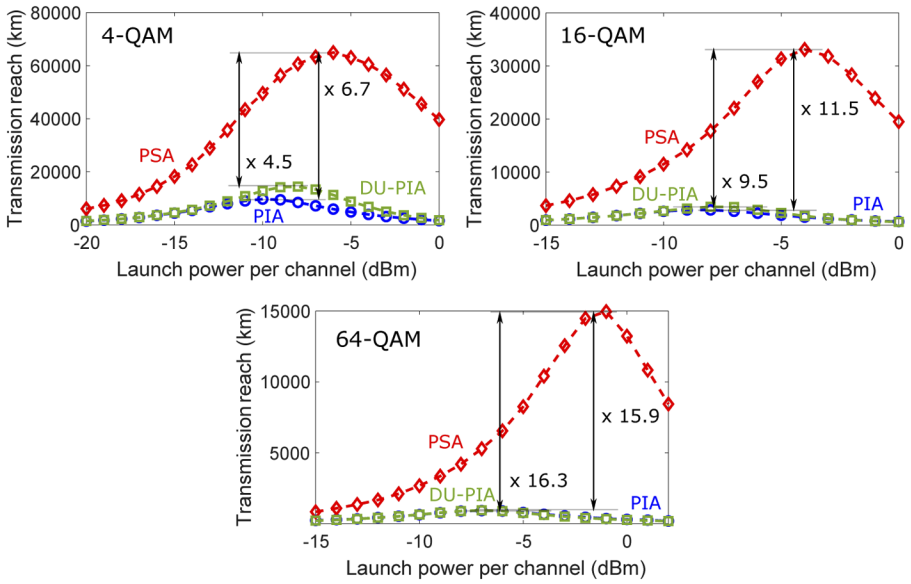

(a) Single-channel system - The dashed blue lines with circle markers, the dashed red lines with diamond markers, and the dashed green lines with square markers correspond to phase-insensitive amplifier (PIA), phase-sensitive amplifier (PSA), and dispersion-unmanaged (DU) PIA links, respectively. The top-left figure is for 4-QAM, top-right for 16-QAM, and the bottom for the 64-QAM. The vertical lines with arrows indicate the maximum transmission reach increase (MTRI).

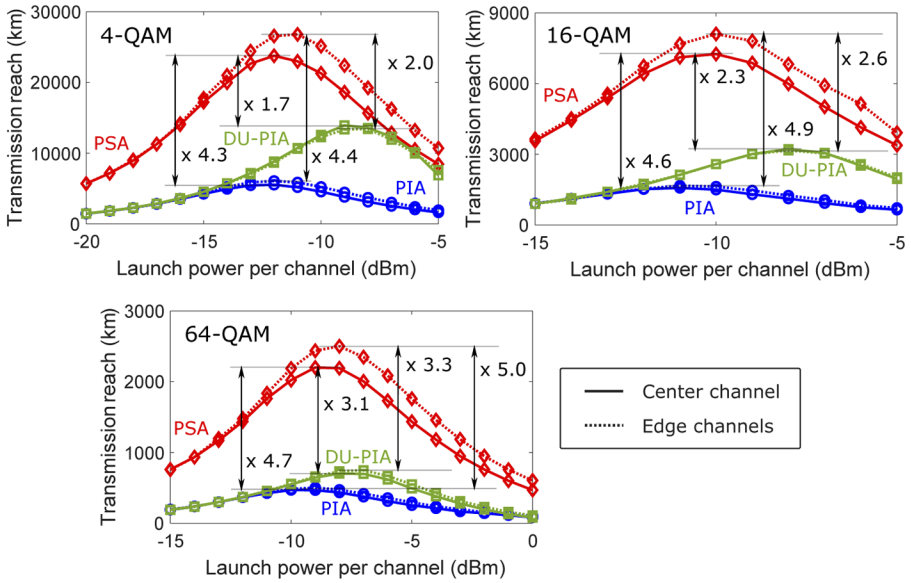

(b) Multi-channel system - The blue lines with circle markers, the red lines with diamond markers, and the green lines with square markers correspond to phase-insensitive amplifier (PIA), phase-sensitive amplifier (PSA), and dispersion-unmanaged (DU) PIA links, respectively. The dotted lines represent the edge channels, and the solid lines represent the center channel. The top-left figure is for 4-QAM, top-right for 16-QAM, and the bottom for 64-QAM. The vertical lines with arrows indicate the maximum transmission reach increase (MTRI).

Fig. 5. Simulation results - Transmission reach versus the launch power, P_{IN} for the multi-span links.

Optics EXPRESS

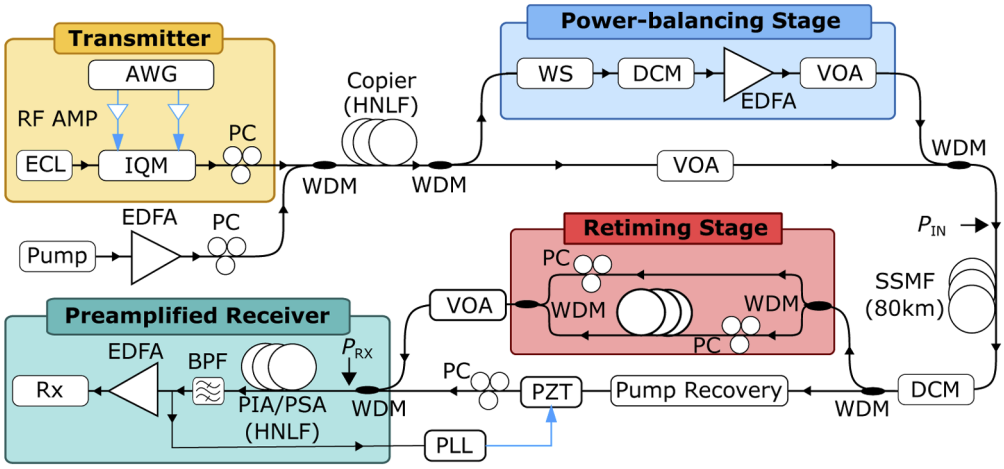

Fig. 6. Experimental setup used for single-span fiber transmission with phase-(in)sensitive amplifiers as preamplifiers: ECL - External-cavity laser, AWG - Arbitrary waveform generator, RF AMP - Radio-frequency amplifier, IQM - IQ modulator, PC - Polarization controller, EDFA - Erbuim-doped fiber amplifier, WDM - Wavelength-division-multiplexing coupler, WS - WaveShaper, DCM - Dispersion compensation module, VOA - Variable optical attenuator, SSMF - Standard single-mode fiber, PZT - Piezoelectric transducer, PIA - Phase-insensitive amplifier, PSA - Phase-sensitive amplifier, BPF - Optical bandpass filter, Rx - Coherent receiver.

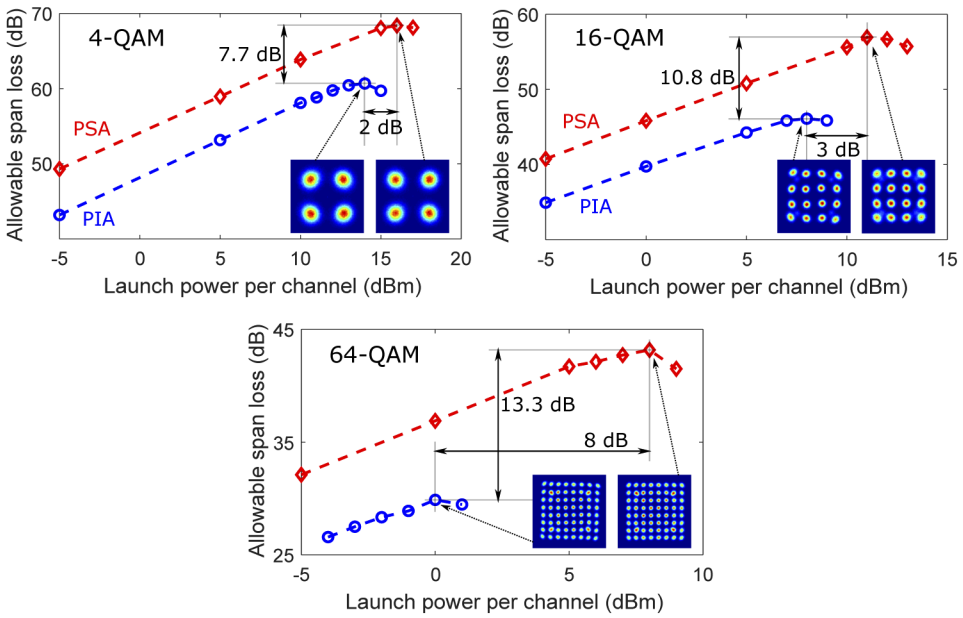

Fig. 7. Experimental results - Allowable span loss versus the launch power, P_{IN} for single-span links. The dotted blue lines and the solid red lines correspond to phase-insensitive amplifier (PIA) and phase-sensitive amplifier (PSA) links, respectively. The top-left figure is for 4-QAM, top-right for 16-QAM, and the bottom for the 64-QAM. Inset: Constellation diagrams at optimum launch powers for PIAs and PSAs with different modulation formats.

Optics EXPRESS

or DU-PIA link. The MTRI for PSAs compared to PIAs or DU-PIAs are also marked in the subfigures of Fig. 7 for different modulation formats. For the PIA, only a few spans were propagated before reaching BER of $2\text{x}10^{-3}$ with a 256-QAM signal. Therefore, the 256-QAM modulation format is not included in the multi-span study. Also, for the multi-span links, the MTRI is enhanced when using PSAs compared to PIAs with higher-order modulation formats due to nonlinearity mitigation.

4. Experiments

4.1. Experimental setup

A proof-of-concept experiment was performed to verify the transmission reach increase dependence on modulation formats in PSA links. An experimental setup as shown in Fig. 6 was used. An external cavity laser (ECL) set at 1550.1nm was used as the signal source, modulated at 10 GBaud using an IQ modulator (IQM) driven by the amplified electrical signals from an arbitrary waveform generator (AWG). The electrical signal was made of 2^{15} randomly generated symbols, which were shaped electrically with an RRC filter of 0.1 roll-off. For 16-QAM and 64-QAM modulation formats, the electrical signal included 4-QAM pilots for assisting digital signal processing (DSP) at the receiver leading to an additional overhead of 6.2%. A high power pump at 1554.1 nm of around 28 dBm was combined with the signal and fed into the first HNLF (the copier). Any further increase of pump power leads to penalties in the signal performance from stimulated Brillouin scattering (SBS). The copier produced an idler at 1558.1 nm, which is a conjugated copy of the signal through the process of four-wave mixing (FWM). A strained HNLF of 150 m was used as the copier.

After the copier, the pump was separated from the signal and idler waves. The signal and idler waves were power balanced using a waveshaper (WS) for the PSA. For phase-insensitive operation, the idler was blocked in the WS. After the WS, a tunable fiber-Bragg grating (FBG) based dispersion compensation module (DCM) was used for dispersion pre-compensation. A low-noise EDFA was used to amplify the signal and idler followed by a variable optical attenuator (VOA) to set the required launch power, P_{IN} into the transmission span. The strong pump was attenuated to about 1 dBm to avoid nonlinearities in the transmission span. The attenuated pump, along with the signal and idler were copropagated in the span. An 80-km standard single-mode fiber (SSMF) was used as the transmission span. Another FBG based DCM was used for dispersion post-compensation. At high launch powers, the signal and idler experiences correlated nonlinear distortions. The two tunable DCMS were used to set the required pre- and post-dispersion compensation for better nonlinearity mitigation in the PSA. The weak pump was separated from the signal and idler and regenerated for phase-sensitive amplification with optical injection locking. The path-length-matching fibers and variable-delay line (VDL) were used to temporally realign the signal and idler compensating for the group delay difference. Another VOA was used after the retiming stage to set the received power, P_{RX} at the preamplifier input. The second HNLF acts as the PIA/PSA. The pump power into the second HNLF was set around 30 dBm, limited by the SBS threshold. The second HNLF consisted of four different spools of strained HNLF with a total length of about 600 m. These spools were spliced together with isolators in between to suppress the SBS. A piezoelectric transducer (PZT) with a phase-locked loop (PLL) was used to stabilize the PSA as well as to maximize the PSA output signal power. A 40-kHz tone from the PLL was used to dither the pump with the help of the PZT. The dithering tone was transferred from the pump to the signal in the PSA. After the PSA, the 40-kHz tone was recovered from the signal and was used as the feedback to the PLL. The PSA had a gain of 22 dB compared to 16 dB for the PIA, simultaneously providing 6-dB improvement in the signal NF [16] and mitigating Kerr nonlinearities at high launch power. The pre- and post-dispersion compensation was optimized for best performance for all the configurations experimentally. For

Optics EXPRESS

the PSA, the optimized ratio of pre- to post-dispersion compensation was 26.7% for all the modulation formats.

After the PSA, the signal was filtered and sent to the receiver, where the BER was calculated. At the receiver, the QAMpy package [37] was used for DSP. The sensitivity, i.e., the P_{RX} required, was measured at BER = $2x10^{-3}$. The P_{IN} and P_{RX} correspond to only the signal powers at the span input and preamplifier input, respectively.

4.2. Experimental results

For 4-, 16-, and 64-QAM, P_{IN} was varied, and the sensitivity was measured. The allowable span loss was calculated from the difference between the P_{IN} and sensitivity, similar to the simulations. The allowable span loss is plotted versus the P_{IN} for both the PIA and PSA in Fig. 7 for different modulation formats. The top-left, top-right, and bottom figures correspond to 4-, 16-, and 64-QAM, respectively. Similar trends to the simulation results were observed. The experimental results are also summarized in Table 3. In the case of the 4- and 16-QAM, we obtain the allowable span loss increase using PSA to be around 6 dB compared to PIA in the linear regime at low launch powers. Due to SNR limitations, it was not possible to measure 64-QAM in the linear regime. The 6-dB improvement comes from the low-noise amplification of the PSA [16]. From low-noise amplification and nonlinearity mitigation, we obtain the MASL increase of 7.7, 10.8, and 13.3 dB for 4-, 16-, and 64-QAM, respectively. It can be seen that the experimental results confirm the simulation results of MASL increase enhancement in the single-span and single-channel experiment.

Table 3. Summary for the single-span link experiments: PIA - Phase-insensitive amplifier, PSA - Phase-sensitive amplifier, OLP - Optimum launch power, MASL - Maximum allowable span loss, OLP increase = $OLP_{PSA} - OLP_{PIA}$, MASL increase = $MASL_{PSA} - MASL_{PIA}$.

Modulation format	PIA		PSA		OLP increase (dB)	MASL increase (dB)
	OLP (dBm)	MASL (dB)	OLP (dBm)	MASL (dB)		
4-QAM	14.0	60.7	16.0	68.4	2.0	7.7
16-QAM	8.0	46.1	11.0	56.9	3.0	10.8
64-QAM	0.0	29.9	9.0	43.2	9.0	13.3

The constellation points at optimum launch powers for both the PIAs and the PSAs corresponding to a BER of around $2x10^{-3}$ are shown in the insets of Fig. 7. The nonlinear distortions can be seen in the constellation diagrams of the PIAs. For higher-order modulation formats, the outer constellation points with higher amplitude levels experience larger nonlinearity-induced shifts compared to the inner points. The nonlinear distortions are absent in the constellation diagrams of the PSAs verifying nonlinearity mitigation.

5. Discussion

The phase rotations or distortions caused by nonlinearities depends on the field amplitudes. In the case of higher-order QAM modulation formats, the different amplitude levels undergo different nonlinear phase rotations. Also, in the higher-order modulation formats, smaller phase distortions can result in higher BER. The coherent addition of the signal and idler fields at the PSA converts these phase rotations to amplitude distortions. The enhancement in the transmission reach increase when using the PSAs compared to the PIAs for higher-order modulation formats can be attributed to the effective mitigation of smaller nonlinear phase distortions by the PSA.

In the experiments, after propagation in the transmission span, the signal and idler waves were separated from the weak pump wave. The additional span loss was added by the VOA after the retiming stage only to the signal and idler waves. The weak pump wave took an alternate path,

Optics EXPRESS

and the pump power into the optical injection locking was kept constant. However, in a real system, the additional span loss will also affect the weak pump. There will be a need to recover the pump wave for the PSA from low powers. Recently, optical injection locking was used to recover the pump for the PSA from input powers of -72 dBm [38]. However, doing so will added some penalty to the sensitivity, which in turn will slightly affect the MASL.

In the three-channel system, XPM is the dominant nonlinear effect. PSAs are less effective in mitigating XPM compared to SPM [22]. This is evident from the low MTRI for both the center and edge channels in the multi-span links compared to the single-channel system. However, the transmission reach can be further improved by using modified Volterra nonlinear equalizer (VNLE) in PSA links [28], which, however, is outside the scope of this work. In polarization-division multiplexed systems, cross-polarization modulation (XpolM) is one other dominant nonlinear effect [39], and further work will be needed to establish how well it can be mitigated by PSAs.

The nonlinear distortions experienced by the pulses in the optical fiber also depends on their shape. In this work, RRC pulses were used. Simulations were also performed with non-return-to-zero (NRZ) pulses for a single-span and single-channel system. The MTRI, when using the PSA compared to PIA, was found to be higher for NRZ pulses than RRC for all modulation formats.

The MTRI obtained in the case of the PSAs is at the expense of half the spectral efficiency. The spectral efficiency of PIA/DU-PIA links with 4-QAM is 2 bits/s/Hz and is the same as that of PSA links with a 16-QAM signal. In single-channel, multi-span simulations, when using the 16-QAM modulation format with PSAs, the maximum transmission reach can be extended 229% and 340% compared to DU-PIAs and PIAs with 4-QAM signal for the same spectral efficiency. A similar study was performed for PCTWs experimentally in [7]. However, the DP-16-QAM phase-conjugated twin waves (PCTWs) performed worse than the DP-4-QAM PIA with spectral efficiency of 4 bits/s/Hz due to higher implementation penalties for DP-16-QAM.

In the single-span and single-channel system, the MASL increase was enhanced with higher-order modulation formats in experiments similar to the simulations. However, due to the increasing implementation penalties and subsequent higher nonlinear phase noise [40] for higher-order modulation formats in the experiments, we believe that a higher MASL increase was obtained for higher-order modulation formats compared to the simulations. For the multi-span links, comparing the 4-QAM [25] and 16-QAM [27] experiments, the transmission reach increase for 16-QAM was lower compared to 4-QAM, which is contradictory to our simulation results. This can be attributed to improper working of the PLL in case of the multi-level modulation format in the loop [28] and needs further investigation.

6. Conclusion

Using a higher-order modulation format enhances the transmission reach increase with PSAs compared to PIAs due to the susceptibility of the higher-order modulation formats to small nonlinear distortions and PSA's effectiveness in mitigating these small nonlinear distortions. This has been validated for single- and three-channel systems in single- and multi-span links using MATLAB simulations. A single-channel, single-span experiment with 4-, 16-, and 64-QAM were performed to verify the transmission reach increase enhancement dependence on modulation formats. For the first time, we show a 64-QAM signal transmitted over a phase-sensitively amplified single-span fiber link. The optimum launch powers are increased by 2, 3, and 8 dB in the case of the PSAs for 4- 16-, and 64-QAM, respectively, compared to PIAs verifying nonlinearity mitigation. We also measure the maximum allowable span loss increase to be 7.7, 10.8, and 13.3 dB for 4-, 16-, and 64-QAM respectively from low-noise amplification and nonlinearity compensation.

Optics EXPRESS

Funding

Vetenskapsrådet (2015-00535).

Acknowledgments

The authors would like to thank C. Naveau and J. Schröder for fruitful discussions. We also thank OFS Denmark for providing the HNLFs used for the PSA. The simulations were performed on resources at Chalmers Centre for Computational Science and Engineering (C3SE) provided by the Swedish National Infrastructure for Computing (SNIC).

Disclosures

The authors declare no conflicts of interest.

References

1. A. D. Ellis, J. Zhao, and D. Cotter, "Approaching the non-linear Shannon limit," J. Lightwave Technol. **28**(4), 423–433 (2010).
2. A. D. Ellis, M. E. McCarthy, M. A. Z. A. Khateeb, M. Sorokina, and N. J. Doran, "Performance limits in optical communications due to fiber nonlinearity," Adv. Opt. Photonics **9**(3), 429–503 (2017).
3. E. Ip and J. M. Kahn, "Compensation of dispersion and nonlinear impairments using digital backpropagation," J. Lightwave Technol. **26**(20), 3416–3425 (2008).
4. D. Rafique, M. Mussolin, M. Forzati, J. Mårtensson, M. N. Chugtai, and A. D. Ellis, "Compensation of intra-channel nonlinear fibre impairments using simplified digital back-propagation algorithm," Opt. Express **19**(10), 9453–9460 (2011).
5. S. K. Turitsyn, J. E. Prilepsky, S. T. Le, S. Wahls, L. L. Frumin, M. Kamalian, and S. A. Derevyanko, "Nonlinear Fourier transform for optical data processing and transmission: advances and perspectives," Optica **4**(3), 307–322 (2017).
6. X. Liu, A. Chraplyvy, P. Winzer, R. Tkach, and S. Chandrasekhar, "Phase-conjugated twin waves for communication beyond the Kerr nonlinearity limit," Nat. Photonics **7**(7), 560–568 (2013).
7. X. Liu, S. Chandrasekhar, P. J. Winzer, R. W. Tkach, and A. R. Chraplyvy, "Fiber-nonlinearity-tolerant superchannel transmission via nonlinear noise squeezing and generalized phase-conjugated twin waves," J. Lightwave Technol. **32**(4), 766–775 (2014).
8. R. A. Fisher, B. R. Suydam, and D. Yevick, "Optical phase conjugation for time-domain undoing of dispersive self-phase-modulation effects," Opt. Lett. **8**(12), 611–613 (1983).
9. W. Pieper, C. Kurtzke, R. Schnabel, D. Breuer, R. Ludwig, K. Petermann, and H. G. Weber, "Nonlinearity-insensitive standard-fibre transmission based on optical-phase conjugation in a semiconductor-laser amplifier," Electron. Lett. **30**(9), 724–726 (1994).
10. S. L. I. Olsson, B. Corcoran, C. Lundström, T. A. Eriksson, M. Karlsson, and P. A. Andrekson, "Phase-sensitive amplified transmission links for improved sensitivity and nonlinearity tolerance," J. Lightwave Technol. **33**(3), 710–721 (2015).
11. R. Tang, J. Lasri, P. S. Devgan, V. Grigoryan, P. Kumar, and M. Vasilyev, "Gain characteristics of a frequency nondegenerate phase-sensitive fiber-optic parametric amplifier with phase self-stabilized input," Opt. Express **13**(26), 10483–10493 (2005).
12. C. M. Caves, "Quantum limits on noise in linear amplifiers," Phys. Rev. D **26**(8), 1817–1839 (1982).
13. R. Tang, P. Devgan, P. L. Voss, V. S. Grigoryan, and P. Kumar, "In-line frequency-nondegenerate phase-sensitive fiber-optical parametric amplifier," IEEE Photonics Technol. Lett. **17**(9), 1845–1847 (2005).
14. I. Bar-Joseph, A. Friesem, R. Waarts, and H. Yaffe, "Parametric interaction of a modulated wave in a single-mode fiber," Opt. Lett. **11**(8), 534–536 (1986).
15. K. J. Lee, F. Parmigiani, S. Liu, J. Kakande, P. Petropoulos, K. Gallo, and D. Richardson, "Phase sensitive amplification based on quadratic cascading in a periodically poled lithium niobate waveguide," Opt. Express **17**(22), 20393–20400 (2009).
16. Z. Tong, C. Lundström, P. Andrekson, C. McKinstrie, M. Karlsson, D. Blessing, E. Tipsuwannakul, B. Puttnam, H. Toda, and L. Grüner-Nielsen, "Towards ultrasensitive optical links enabled by low-noise phase-sensitive amplifiers," Nat. Photonics **5**(7), 430–436 (2011).
17. J. Yang, M. Ziyadi, Y. Akasaka, S. Khaleghi, M. R. Chitgarha, J. Touch, and M. Sekiya, "Investigation of polarization-insensitive phase regeneration using polarization-diversity phase-sensitive amplifier," in *European Conference and Exhibition on Optical Communication (ECOC 2013)*, (2013), pp. 1–3.
18. T. Umeki, T. Kazama, O. Tadanaga, K. Enbutsu, M. Asobe, Y. Miyamoto, and H. Takenouchi, "PDM signal amplification using PPLN-based polarization-independent phase-sensitive amplifier," J. Lightwave Technol. **33**(7), 1326–1332 (2015).

Optics EXPRESS

19. A. Lorences-Riesgo, C. Lundström, F. Chiarello, M. Karlsson, and P. A. Andrekson, "Phase-sensitive amplification and regeneration of dual-polarization BPSK without polarization diversity," in *2014 The European Conference on Optical Communication (ECOC)*, (2014), pp. 1–3.
20. A. Lorences-Riesgo, T. A. Eriksson, C. Lundström, M. Karlsson, and P. A. Andrekson, "Phase-sensitive amplification of 28 GBaud DP-QPSK signal," in *Optical Fiber Communication Conference*, (Optical Society of America, 2015), p. W4C.4.
21. N. Rossi, P. Serena, and A. Bononi, "Symbol-rate dependence of dominant nonlinearity and reach in coherent WDM links," J. Lightwave Technol. **33**, 1 (2015).
22. K. Vijayan, B. Foo, M. Karlsson, and P. A. Andrekson, "Cross-phase modulation mitigation in phase-sensitive amplifier links," IEEE Photonics Technol. Lett. **31**(21), 1733–1736 (2019).
23. C. E. Shannon, "A mathematical theory of communication," Bell Syst. Tech. J. **27**(3), 379–423 (1948).
24. B. Corcoran, S. L. I. Olsson, C. Lundström, M. Karlsson, and P. Andrekson, "Phase-sensitive optical pre-amplifier implemented in an 80km DQPSK link," in *OFC/NFOEC*, (2012), pp. 1–3.
25. S. L. Olsson, H. Eliasson, E. Astra, M. Karlsson, and P. A. Andrekson, "Long-haul optical transmission link using low-noise phase-sensitive amplifiers," Nat. Commun. **9**(1), 2513 (2018).
26. S. L. Olsson, T. A. Eriksson, C. Lundström, M. Karlsson, and P. A. Andrekson, "Linear and nonlinear transmission of 16-QAM over 105 km phase-sensitive amplified link," in *Optical Fiber Communication Conference*, (Optical Society of America, 2014), p. Th1H.3.
27. S. L. I. Olsson, M. Karlsson, and P. A. Andrekson, "Long-haul optical transmission of 16-QAM signal with in-line phase-sensitive amplifiers," in *2017 European Conference on Optical Communication (ECOC)*, (2017), pp. 1–3.
28. B. Foo, M. Karlsson, K. Vijayan, M. Mazur, and P. A. Andrekson, "Analysis of nonlinearity mitigation using phase-sensitive optical parametric amplifiers," Opt. Express **27**(22), 31926–31941 (2019).
29. K. Vijayan, Z. He, B. Foo, M. Karlsson, and P. A. Andrekson, "Nonlinearity mitigation dependence on modulation format in phase-sensitively amplified fiber links," in *Frontiers in Optics / Laser Science*, (2020).
30. ITU-T G.975.1, (2004).
31. Z. Liu and R. Slavík, "Optical injection locking: From principle to applications," J. Lightwave Technol. **38**(1), 43–59 (2020).
32. R. Kakarla, J. Schröder, and P. A. Andrekson, "Optical injection locking at sub nano-watt powers," Opt. Lett. **43**(23), 5769–5772 (2018).
33. K. Vijayan, B. Foo, H. Eliasson, and P. A. Andrekson, "Cross-phase modulation mitigation in WDM transmission systems using phase-sensitive amplifiers," in *European Conference on Optical Communication (ECOC)*, (2018), pp. 1–3.
34. K. Vijayan, B. Foo, M. Karlsson, and P. A. Andrekson, "Long-haul transmission of WDM signals in with in-line phase-sensitive amplifiers," in *2019 European Conference on Optical Communication (ECOC)*, (2019), pp. 1–3.
35. B. Corcoran, S. L. I. Olsson, C. Lundström, M. Karlsson, and P. A. Andrekson, "Mitigation of nonlinear impairments on QPSK data in phase-sensitive amplified links," in *39th European Conference and Exhibition on Optical Communication (ECOC 2013)*, (2013), pp. 1–3.
36. G. P. Agrawal, *Nonlinear fiber optics* (Elsevier / Academic Press, 2013).
37. J. Schröder and M. Mazur, "QAMPy a DSP chain for optical communications, DOI: 10.5281/zenodo.1195720,".
38. R. Kakarla, J. Schröder, and P. A. Andrekson, "One photon-per-bit receiver using near-noiseless phase-sensitive amplification," Light: Sci. Appl. **9**(1), 153–157 (2020).
39. A. Bononi, P. Serena, N. Rossi, and D. Sperti, "Which is the dominant nonlinearity in long-haul PDM-QPSK coherent transmissions?" in *36th European Conference and Exhibition on Optical Communication*, (2010), pp. 1–3.
40. S. L. Olsson, M. Karlsson, and P. A. Andrekson, "Nonlinear phase noise mitigation in phase-sensitive amplified transmission systems," Opt. Express **23**(9), 11724–11740 (2015).